

**Anisotropy of surface optical properties at BN(110): An *ab initio* study**

Giancarlo Cappellini and Guido Satta

*INFM Sezione di Cagliari and Dipartimento di Fisica, Università di Cagliari, Cittadella Universitaria, Strada Provinciale Monserrato-Sestu Km 0.700, I-09042 Monserrato (Ca), Italy*

Maurizia Palummo and Giovanni Onida\*

*INFM Sezione di Roma-2 and Dipartimento di Fisica, Università di Tor Vergata, via della Ricerca Scientifica 1, I-00133 Rome, Italy*

(Received 5 March 2002; revised manuscript received 10 June 2002; published 24 September 2002)

We present a calculation of the linear optical properties of the nonpolar (110) surface of cubic boron nitride, performed within the first-principle density-functional theory and local-density approximation scheme. The reflectance anisotropy (RA) spectrum is analyzed in relation to the better known spectrum of the GaAs(110) surface and to the existing tight-binding results for GaN(110). Previous results for the RA spectrum of GaN(110) obtained in tight-binding scheme are here confirmed, including a negative structure at the onset. For BN(110) the present first *ab initio* results show the fundamental role played by surface-states transitions at the onset of the RA spectrum. The origin of the optical structures is studied in comparison with the RA spectra of GaAs(110) and GaN(110), in connection with the differences in ionicity between nitrides and GaAs, and considering the specific relaxation occurring at nitrides (110) surfaces.

DOI: 10.1103/PhysRevB.66.115412

PACS number(s): 78.20.Bh, 78.68.+m, 73.20.At, 71.15.Mb

**I. INTRODUCTION**

In recent years BN and GaN, among other III-V semiconductors, have attracted much attention for their very peculiar electronic properties. Their hardness, high melting point, and large bulk moduli make them ideal as protective coating materials.<sup>1,2</sup> Besides that, other properties such as the high thermal conductivity, wide band gap, and low dielectric constant are very attractive for applications in optical and electronic devices.<sup>1-3</sup> In fact, nitride semiconductors are visible light emitters and detectors, hence have gained importance due to their real and potential applications.

Modern semiconductor devices in general consist of many layers (planar and nonplanar) of different materials, grown usually by epitaxial processes such as the molecular-beam epitaxy.<sup>4</sup> Different techniques have been therefore employed to probe the growth mechanisms and the structure of surfaces. Between the most successful tools used for this goal are surface sensitive optical techniques, which permit nondestructive *in situ* measurements over a broad range of operating environments and in real time. The study of optical properties of surfaces is therefore a rapidly developing field of research, because of the versatility and nondamaging character of the optical measurements. The comparison between measured and calculated spectra has yielded information on atomic and electronic structure of many surfaces.<sup>5</sup>

The properties of boron nitride (BN) have motivated detailed theoretical and experimental studies since a long time.<sup>6-8</sup> Many advanced technologies rely on boron nitride and on materials based on it, due to the wide spectrum of properties offered by its polymorphic modifications, two graphitelike and two dense ones. Boron nitride shares many of its properties, structures, processings, and applications with carbon. Cubic boron nitride (also known as sphalerite boron nitride and abbreviated as Z-BN, *c*-BN, or  $\beta$ -BN), with  $sp^3$ -hybridized B—N bonds, has the diamond crystal structure and a similar lattice constant. Its physical proper-

ties, such as extreme hardness, wide energy band gap, low dielectric constant, and high thermal conductivity, are also very near to those of diamond. These remarkable properties of *c*-BN have many appealing applications in modern microelectronic devices, and make it useful also as a protective coating material or in high-duty tools.<sup>2</sup> Moreover, the possibility to grow BN nanotubes has stimulated a large interest upon the layered hexagonal phase (*h*-BN) too.<sup>9</sup>

It is now generally agreed experimentally that bulk *c*-BN is the thermodynamically stable phase at ambient conditions, and that the less dense *h*-BN becomes stable at temperatures exceeding  $T \sim 1200$  K.<sup>10</sup> Since 1979 *c*-BN chemical vapor deposited films have been realized,<sup>11</sup> but the production of pure *c*-BN thin films (either by chemical or physical vapor deposition) remains a difficult task due to the formation, during the growth process, of unwilling *h*-BN domains.<sup>12</sup> A general consensus gained from the experimental excitation energies is that the minimum band gap is direct in the case of *h*-BN, and indirect in the case of *c*-BN. For *h*-BN a direct band gap of  $5.2 \pm 0.2$  eV associated to the transition  $H_{3v}-H_{2c}$  has been estimated,<sup>13</sup> while a value of  $6.4 \pm 0.5$  eV for the indirect minimum band gap in *c*-BN has been determined,<sup>14</sup> and associated to the  $\Gamma_{15v}-X_{1c}$  transition.<sup>15,16</sup> *Ab initio* linear optical functions of *c*- and *h*-BN, studied within density-functional theory and local-density approximation (DFT-LDA) and GW schemes, have been addressed by us in a previous work.<sup>17</sup>

In the present paper, we study the optical reflectance anisotropy of the (110) surface of cubic BN and compare it to that of GaAs and GaN. Reflectance anisotropy spectroscopy (RAS) involves the interaction of polarized electromagnetic radiation with the surface (and bulk) electronic dipole moments. With this technique, one measures the difference in reflectivity between two orthogonal polarizations of light at near-normal incidence. When applied to the surface of an isotropic bulk crystal (such as cubic BN, GaN, and GaAs), there is no net contribution from the bulk. Under these con-

ditions, the RAS signal arises from the symmetry reduction at the surface, with respect to the bulk, caused by crystal termination and by the surface reconstruction or relaxation.<sup>5,18</sup>

Other surfaces of BN have been studied previously using ultrasoft pseudopotential schemes. The nonpolar *c*-BN(001) differently reconstructed surfaces have been systematically studied with respect to their stability, structure, and electronic excitations.<sup>19,20</sup> On the other hand, the stability of different reconstructions of the polar (111) and ( $\bar{1}\bar{1}\bar{1}$ ) surfaces of *c*-BN has been already addressed.<sup>21,22</sup> In the present paper, we study the (110) surface of BN in comparison with the same surface of GaN and GaAs. It shows a simpler relaxation pattern with respect to other more complicated reconstructed surfaces of *c*-BN.<sup>19,20</sup> Moreover, the GaAs(110) nonpolar surface has been widely studied previously with respect to its structural and optical properties by two authors of the present collaboration.

The optical properties of the nonpolar (110) surface of cubic boron nitride have been studied starting from a surface electronic structure calculation within the *ab initio* DFT-LDA scheme. We calculated the imaginary part of the dielectric function and the reflectance anisotropy spectrum.<sup>23</sup> In parallel, we analyzed the results relative to the better known GaAs(110) surface as well. Indeed GaAs(110) can be considered as a prototype of the III-V(110) surface relaxation. Moreover, calculations within the same scheme have been here performed also for GaN(110), comparing the results with existing tight-binding (TB) data for this surface.<sup>24</sup> The RAS signal for GaN(110) shows a negative structure at the onset, in contrast to what happens in GaAs(110). The tight-binding optical results for GaN(110) are confirmed by our DFT-LDA pseudopotential calculation.<sup>24</sup> For BN(110), we present here the first *ab initio* optical properties calculation. For this system, we address in detail the role of transitions involving surface states at the onset.

The paper is organized as follows. In Sec. II, we give the computational details and ground-state properties of the considered surfaces. In Sec. III, we describe the theoretical scheme used to evaluate the optical properties. In the same section we report the RA spectra relative to all the considered surfaces, and we discuss the results. The origin of the optical features in the spectra at the (110) nitrides surfaces is then addressed. Finally, conclusions are drawn in Sec. IV.

## II. STRUCTURAL PROPERTIES OF BN(110) AND COMPUTATIONAL DETAILS

Density-functional calculations have been carried out within the local-density approximation for the exchange and correlation functional,<sup>25</sup> using the Perdew and Zunger parametrization<sup>26</sup> of Ceperley and Alder results.<sup>27</sup> Kohn-Sham orbitals are expanded in a plane-wave basis set, with an energy cutoff of 55 Ry. Care has been used in constructing the ionic pseudopotentials, in order to avoid the occurrence of ghost states and to ensure an optimal transferability.<sup>28,29</sup> Angular components up to  $l=2$  have been included. Separable, norm-conserving soft pseudopotentials have been generated within the scheme of Troullier and Martins,<sup>30</sup> with the

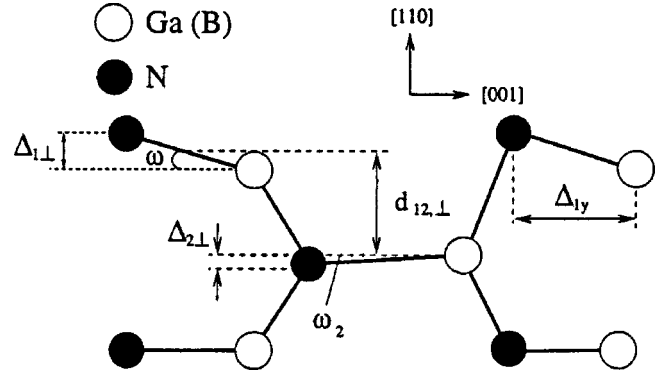


FIG. 1. Structure of BN(110) and GaN(110) surfaces after Ref. 34. Side view and relaxation parameters. See also Refs. 35,36.

following core radii (bohr): 1.59 (B,  $3d$ ), 1.49 (N,  $2p$ ). For boron, nonlinear core corrections (NLCC), to be used in the solid calculation, have been taken into account in generating pseudopotentials and pseudo-wave-functions.<sup>31</sup> In the case of GaN an energy cutoff of 40 Ry has been used, and NLCC have been considered for the Ga atom. A lower energy cutoff (18 Ry) is used for GaAs(110).<sup>32</sup>

In all the cases considered here the bulk crystals are optically isotropic. The semi-infinite solid is replaced by periodically repeated slabs to simulate the real surface. In order to achieve a good convergence of the results we use a system containing eleven atomic layers, with four empty layers to separate adjacent slabs. Convergence in sampling the irreducible surface Brillouin zone (SBZ) for the ground-state calculation is achieved with the use of four special  $\vec{k}$  points.<sup>33</sup> The cleaved (110) surface of zinc-blende materials retains the primitive ( $1 \times 1$ ) periodicity and presents a well-known relaxation pattern. At the surface layer the anion moves away from the bulk, favoring the  $p$  bonding with three neighboring cations, while the surface cation moves into the bulk favoring an  $sp^2$  binding with three neighboring anions.<sup>18,23,34-36</sup> In Fig. 1, a picture of the relaxed (110) surface is shown for BN and GaN after Ref. 34. The surface dimer rotation angle  $\omega$  and dimer bond contraction  $C_B$  for the three surfaces under study are given in Table I, in comparison with the previous data. For the nitride surfaces an *anomalous* behavior results. Rotational angles are nearly halved with respect to GaAs and the bond contractions are appreciable, while they are negligible for GaAs. This behavior can be ascribed to the higher bond ionicity of the III nitrides.<sup>35,36</sup> A quantitative analysis of this point in term of electronegativity, charge transfer per dimer, and charge asymmetry coefficient has already been given, relative to the nonpolar surfaces of nitrides, in a previous work.<sup>35</sup> More-

TABLE I. Dimer rotation angle and bond contraction for the surfaces under study in comparison with previous results. GaAs(I) and GaN(II) from Ref. 35, BN(III) from Ref. 36.

(110)Surface	GaAs(I)	GaAs	GaN(II)	GaN	BN(III)	BN
$\omega$ (deg)	30.1	29.9	14.3	13.0	15.74	15.73
$C_b$ (%)	0.9	1.3	4.9	5.7	7.8	10.4

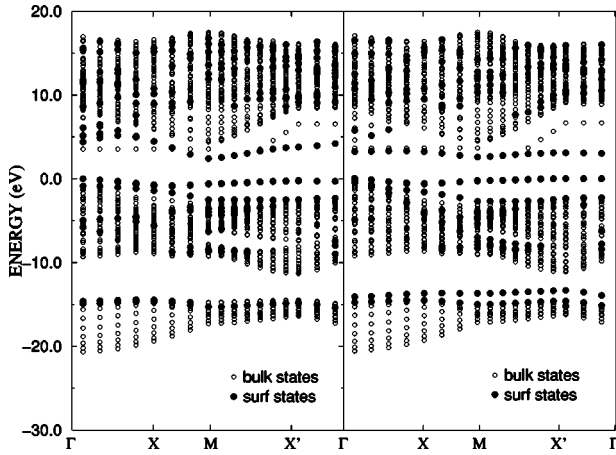


FIG. 2. DFT-LDA band structure of the BN(110) surface in the SBZ. Left panel: relaxed surface. Right panel: band structure for the ideal surface.

over, the structural results obtained with explicit inclusion of the Ga  $d$  electrons in the valence<sup>37</sup> are in very good agreement with those obtained using NLCC, and leaving the Ga  $d$  electrons frozen in the core as we do in the present work. In Fig. 2, the calculated DFT-LDA energy bands in the SBZ have been depicted for the BN ideal and relaxed (110) surfaces. One finds two surface states within the bulk gap: the  $A_5$  state, above the valence-band top, which is the occupied anionic dangling bond (almost unaffected by the surface relaxation); and the state  $C_3$ , below the conduction bands, which is the cationic empty dangling bond experiencing an upward shift after relaxation. This relaxation pattern is common to the (110) surfaces of GaN(110) and GaAs(110). In BN(110), notice that the band gap at  $\Gamma$  is between bulk states. Along  $\bar{X}\Gamma-\bar{\Gamma}$  and  $\bar{M}-\bar{X}\Gamma$  directions the surface bands penetrate inside the band gap even after relaxation. For GaAs(110) a much larger dispersion occurs along these directions of the SBZ,<sup>18,23,38</sup> taking into account the smaller value of the bulk band gap. From Fig. 2 it is clear that dispersion for the states  $A_5$  and  $C_3$  is smaller along  $\bar{\Gamma}-\bar{X}\Gamma$  and  $\bar{M}-\bar{X}\Gamma$  directions with respect to the other directions reported. This finding is in accordance with the bands obtained within other *ab initio* DFT-LDA calculations using non-norm-conserving Vanderbilt pseudopotentials<sup>36</sup> (in the present paper the directions in reciprocal space have been reported with inverted directions with respect to those of Ref. 36).

### III. SURFACE OPTICAL PROPERTIES AND ELECTRONIC EXCITATIONS

A fundamental ingredient for the calculation of the optical properties of the (110) surface is the bulk dielectric function. We determine the bulk optical properties by calculating the momentum matrix elements (MME) associated with dipole transitions at a large number of  $k$  points in the Brillouin zone (BZ). The frequency-dependent imaginary part of the dielectric function is given by<sup>32,39</sup>

$$\epsilon_b^{(2)}(\omega) = \frac{8\pi^2 e^2}{\omega^2 m^2 V} \sum_{v,c} \sum_{\vec{k}} |\langle v, \vec{k} | p_\alpha | c, \vec{k} \rangle|^2 \delta(E_c(\vec{k}) - E_v(\vec{k}) - \hbar\omega), \quad (1)$$

where  $v$  and  $c$  label the valence and conduction states associated with the energies  $E_v(\vec{k})$ ,  $E_c(\vec{k})$ ,  $V$  is the crystal volume,  $\langle \rangle$  is the matrix element of the momentum operator and  $\alpha = x, y, z$ . The sum over  $\vec{k}$  is extended over the bulk BZ of the crystal. In the presence of a nonlocal ionic potential, the momentum operator in Eq. (1), should be replaced by the velocity operator.<sup>40</sup> However, it has been shown that in III-V semiconductors this has a negligible influence on the RA spectra.<sup>41</sup> The eigenvalues and eigenfunctions appearing in Eq. (1), are those determined within the DFT-LDA scheme. As it appears from Eq. (1), local-field effects are also neglected in the dielectric function calculation.<sup>41</sup>

As is well-known, DFT-LDA band structures for semiconductors and insulators do not reproduce the real (experimental) ones. DFT-LDA eigenvalues, when interpreted as the quasiparticle (QP) energies show the so-called *band-gap problem*.<sup>42</sup> The QP energies correspond only qualitatively to the DFT-LDA ones, mainly because the band gaps between conduction and valence bands show a systematic underestimation with respect to the experiments.<sup>43-45</sup> This problem can be solved within a self-energy approach, called GW.<sup>46</sup> Within this method, the self-energy operator reads  $\Sigma = GW$ , where  $G$  is the one-electron Green function and  $W$  the screened Coulomb interaction in the system, fully taking into account the screening properties of the material.<sup>42,46,47</sup> This method has been applied to semiconductors surfaces too.<sup>23</sup> However, we maintain here the calculation of the optical properties at a DFT-LDA level, and we shall comment in the following on the reliability of the DFT-LDA scheme to tackle the issues considered in this work.

Within the slab geometry the RA spectrum can be written as<sup>5,18,38</sup>

$$\frac{\Delta R}{R} = \frac{R_{[\bar{1}10]} - R_{[001]}}{R_o} = \frac{16\pi\omega d}{c} \text{Im} \left[ \frac{\alpha_{[\bar{1}10]}^{hs}(\omega) - \alpha_{[001]}^{hs}(\omega)}{\epsilon_b(\omega) - 1} \right], \quad (2)$$

where  $R_o$  is the average of the two reflectivity signals, and  $\alpha_{ii}^{hs}$  is the half-slab polarizability whose imaginary part reads<sup>18</sup>

$$\alpha_{\gamma\gamma}^{hs(2)}(\omega) = \frac{e^2 \pi}{m^2 \omega^2 A d} \sum_{v,c} \sum_{\vec{k}} |\langle v, \vec{k} | p_\gamma | c, \vec{k} \rangle|^2 \times \delta(E_c(\vec{k}) - E_v(\vec{k}) - \hbar\omega). \quad (3)$$

In Eq. (2),  $\epsilon_b$  is the bulk dielectric function and  $d$  is the half-slab thickness. In Eq. (3),  $A$  is the transverse area of the slab and  $\gamma = x, y, z$ . In the last equation convergence is achieved using 64 special  $\vec{k}$  points in the SBZ and 56 conduction bands. The calculation of  $\alpha$  and  $\epsilon_b$  involves the computation of the matrix elements of the momentum operator between valence and conduction states calculated at the DFT-LDA level. The real parts of the half-slab polarizability

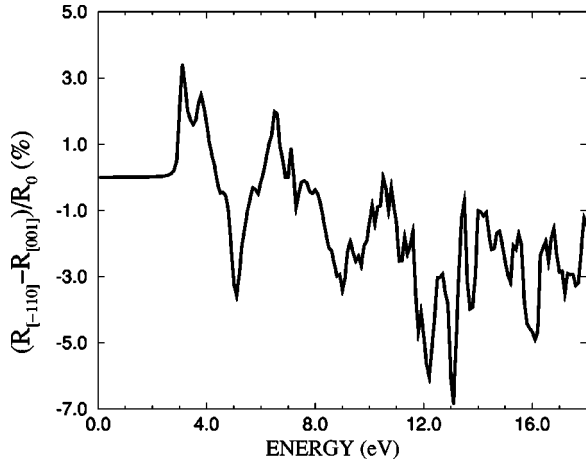


FIG. 3. Calculated RA spectrum of the BN(110) surface.

and the bulk dielectric function have been obtained via the Kramers-Kronig transformations.

In Fig. 3, we report on the calculated reflectance anisotropy spectrum of the BN(110). In the present paper we assume that the  $X$  direction is parallel to the zigzag chains of the (110) surface [i.e.,  $X = (\bar{1}10), Y = (001)$ , in accordance with the literature].<sup>18,24</sup> The RA spectrum, defined therefore as  $(R_X - R_Y)/R_0$ , is dominated at the onset by the reflectivity along the  $X$  direction, with a first positive structure of the order of 2% positioned around 3 eV. This first structure is followed by a sharp negative peak at 5 eV. In Fig. 4, we report on the same quantity obtained in our calculations for GaAs(110) and GaN(110), in comparison with TB data.<sup>24</sup> Our *ab initio* RA spectrum also shows a first negative peak in the GaN(110) case, of the order of 1%. This behavior is different to what happens in GaAs(110). For this system one finds a first positive peak at lower energies in the RA spectrum. For GaN(110) the TB curve of Ref. 24 has been red-shifted to match our DFT-LDA one. The TB calculations in fact do not show the above-mentioned *band-gap problem*, because the results of Ref. 24 have been obtained fitting the

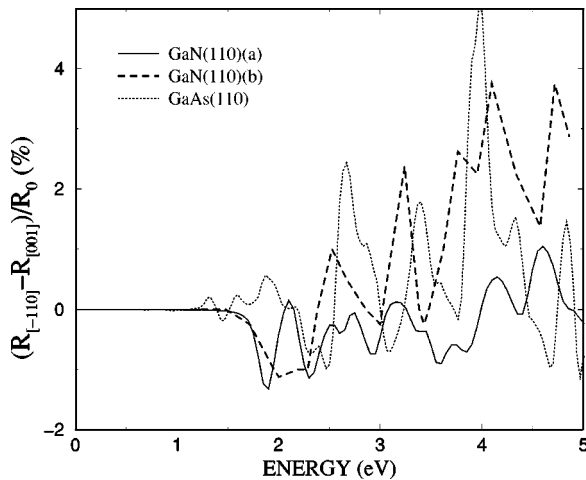


FIG. 4. RA spectra for the (110) surface of GaN (a) and GaAs according to the present calculations. GaN(110)(b) are tight-binding results taken from Ref. 24.

TB parameters to reproduce the experimental optical bulk spectra.<sup>24</sup> The first structure at the RA spectrum for GaAs(110) comes from surface-surface (ss) transitions at  $\bar{X}$  point of the SBZ, and is definitely polarized along the zigzag chain direction.<sup>23,38</sup> On the other hand, in the case of GaN(110) the first negative peak has been assigned in Ref. 24 to surface-bulk (sb) contributions, followed at higher energies by ss transitions. For these transitions the  $Y$  component of the polarizability is larger than the  $X$  one, giving rise to the negative structure in the RA spectrum at low energy for GaN(110). The interplay between sb and ss contributions yields in the TB data a negative *plateau* almost 0.5 eV wide, which follows at higher energies the first negative slope. In Fig. 5 we report on the imaginary part of  $\alpha_{i,i}^{hs}(\omega)$  (times  $4\pi d$ ) for GaN(110) and BN(110), obtained in the present calculations. To gain more insight in the origin of the RA spectra, the different contributions to the transitions have been reported: i.e., ss, sb, bulk-surface (bs), and bulk-bulk (bb).<sup>41</sup> As is clear from this figure, the present *ab initio* results for GaN(110) do assign the low energy structures of the RA spectrum to the sb and the ss transitions. We therefore confirm that sb transitions at onset followed by ss transitions give rise to a  $Y$  component larger than the  $X$  one for the polarizability. In the present calculation the RA spectrum turns out to become slightly greater than zero at 2.2 eV (see Fig. 4). No noticeable *plateau* follows the first negative slope in the RA spectrum in our calculations for GaN(110). On the other hand, a direct correspondence can be drawn for the higher-energy structures in the RA spectra between present results and the TB ones. The sb contributions come from transitions from the anionic  $A_5$  surface state (which is almost flat along the  $\bar{X}-\bar{M}$  direction) to bulk states. The TB results of Ref. 24 with the negative peak occurring at onset in the RA spectrum of GaN(110) due to sb and ss transitions, have been here fully confirmed within the present *ab initio* DFT-LDA approach.

In the case of BN(110), the onset of the RA spectrum is positive and dominated by ss contributions (see Figs. 2 and 3). The energy range of the spectrum is blue shifted with respect to that of GaN(110), due to the larger value of the BN bulk band gap. At about 5 eV the sign of the RA spectrum changes, with ss transitions dominated by the  $Y$  component giving rise to a sharp negative peak. Significant contributions for sb and bs transitions appear above 6 eV. We can ascribe to these transitions the second positive structure around 7 eV. Then, up to 18 eV, the RA spectrum remains negative.

From Fig. 3, it is clear that the first positive structure at onset originates from ss transitions around the  $\bar{M}$  point of the SBZ. In correspondence of that point the minimum gap between  $A_5$  and  $C_3$  surface states for BN(110) occurs. These states, on the other hand, show both an almost flat behavior along the  $\bar{X}'-\bar{\Gamma}$  direction. The first negative structure in the RA spectrum of BN(110) comes from ss transitions along this direction and, in a minor way, from sb near the  $\Gamma$  region. There are noticeable differences arising between RA spectra of BN(110) and GaN(110) at low energy. In GaN(110), an interplay between sb and ss transitions does take place, with the first negative structure due to sb transitions mainly. On

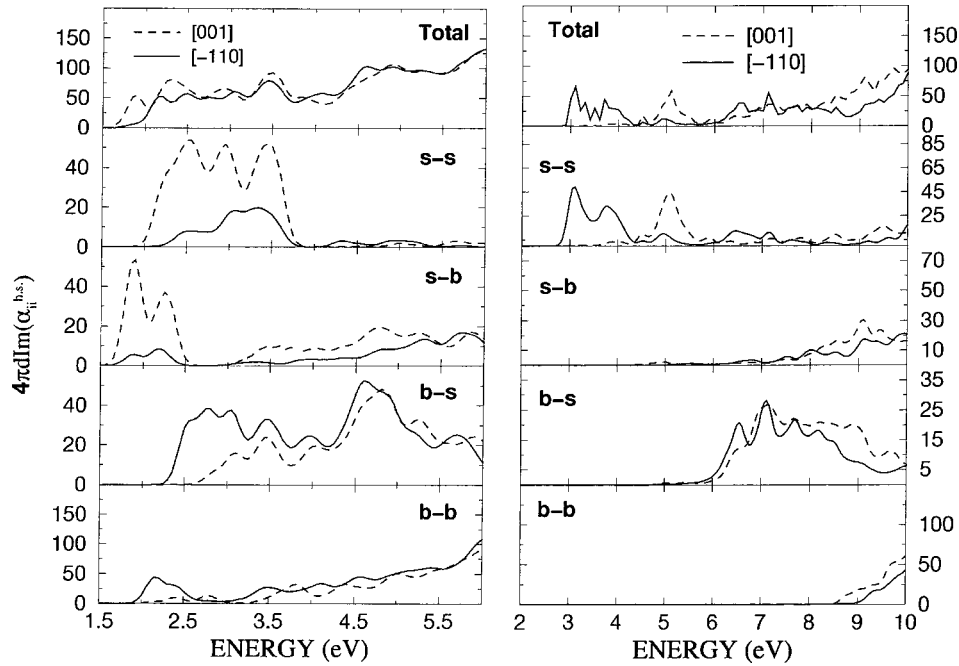


FIG. 5. Calculated imaginary part of the half-slab polarizability for GaN(110) and BN(110)(times  $4\pi d$ ), and components of  $\alpha_{i,i}^{hs}(\omega)$  for different transitions. Solid line:  $\alpha_{x,x}^{hs}(\omega)$ ; dashed line:  $\alpha_{y,y}^{hs}(\omega)$ . Left panel: GaN(110). Right panel: BN(110).

the other hand, in BN(110) the first positive structure and the following sharp negative peak come from ss transitions. The larger strength of the structures present in the optical spectra of the nitrides (110) surfaces, aside from details making the optical response of BN(110) different from that of GaN(110), can be ascribed to the larger ionicity (charge asymmetry) and bond strength (cohesive energy) of the nitrides with respect to the other III-V compounds (e.g., GaAs).

In Fig. 6, we report on the imaginary part of the DFT-LDA bulk dielectric function for *c*-BN and *c*-GaN in a wide energy range. For the case of BN an onset at 8.9 eV appears together with three main structures (A,B,C) which have been found and widely studied in previous works within different computational schemes.<sup>17,48,49</sup> The difference in the energy range is due to the different bulk gap value of the two systems with the  $\epsilon_2$  for *c*-BN blue shifted with respect to that of GaN. In the case of GaN the onset takes place at 2.08 eV, with the three main structures A'(6.8 eV), B'(9.4 eV), and C'(11.7 eV). Aside from little differences, the curve for *c*-GaN reproduces the curve of Fig. 5(a) from the paper by Gavrilenko and Wu.<sup>48</sup> Thus, the bulk optical properties of GaN calculated here within the pseudopotential scheme (with the Ga *d* electrons treated as core ones) are in very good agreement, in a wide energy range, with those calculated within all-electrons free linear augmented plane wave method (FLAPW). Indeed, due to the fact that Ga *d* states do alter mainly the deep valence bands, making interference with N 2*s* states,<sup>50-52</sup> we expect a negligible contribution in the optical low-energy properties. The possible inaccuracies due to the missing explicit contributions of the Ga *d* electrons are not present in the case of BN, whose (110) surface is the main issue addressed in the present paper.

It is of interest to compare the imaginary part of the half-slab polarizability and of the bulk dielectric function for the

same materials in a large spectral range (see Figs. 6 and 7). The high-energy spectrum for GaN(110) slab behaves similarly to the bulk  $\epsilon_2$  with almost no differences between X and Y components of the polarizability. Below 5 eV, transitions involving surface states generate structures with a dominant Y component. On the other hand, for BN(110) at high energy, the X component of the polarizability turns out to be slightly larger than the Y one. The surface states give significant contributions at energies below the bulk band gap, with a dominant X polarization at the onset. The larger bond ionicity of BN with respect to that of GaN determines the larger strength of optical structures in the RA spectra.<sup>35</sup> In fact, the first two structures at the onset for BN(110) (a first positive one followed by a negative peak) are of the order of 3%, while for GaN the first structures (both negative) are of 1%

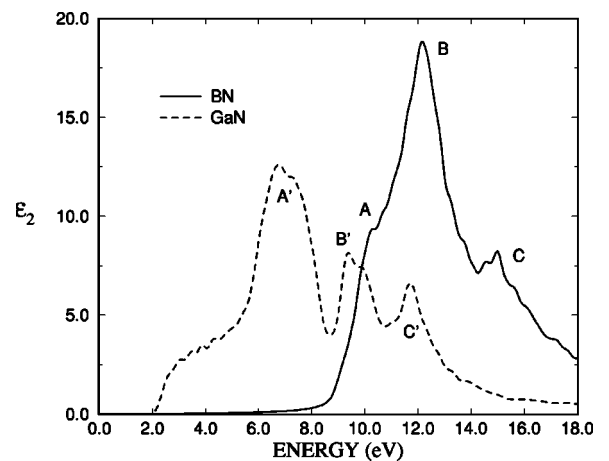


FIG. 6. Imaginary part of the dielectric function for bulk GaN and BN after present calculation.

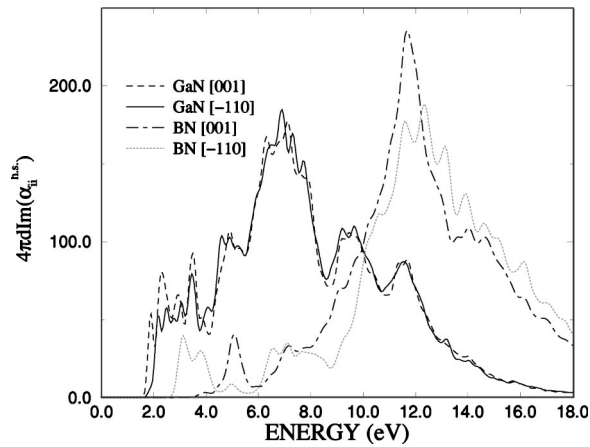


FIG. 7. Calculated imaginary part of the half-slab polarizability for GaN(110) and BN(110)(times  $4\pi d$ ) in a wide spectral range for the two components of  $\alpha_{ii}^{hs}(\omega)$  parallel to the surface.

in magnitude (see Figs. 3 and 4). On the other hand, the RA spectrum of GaAs(110) shows the first two positive peaks having an intensity of one order of magnitude smaller. The more significant strength of optical structures at the onset in the RA spectra for nitrides (110) surfaces can be interpreted as their optical *fingerprints* and can be directly ascribed to their larger ionicity with respect to GaAs.<sup>18,35,36</sup> This is also the origin of the *anomalous* relaxation pattern of their (110) surface.<sup>35,36</sup>

Considering that self-energy corrections<sup>23</sup> and excitonic effects<sup>53</sup> in the RA spectra of semiconductors surfaces consist mainly in energy shifts, we argue that the inclusion of higher-order effects in the calculation of optical properties of

nitrides (110) surfaces will not alter qualitatively the present conclusions. On the other hand, due to the strategic role played by BN and by the other nitrides both in the research and in the technological applications, more refined calculations and experiments on their surface optical properties are highly requested. We plan to go further in the direction of a refinement of the calculations of these systems in the near future.

#### IV. CONCLUSIONS

In conclusion, we have presented optical properties calculations, performed within *ab initio* DFT-LDA, for cubic BN(110) surface. The results have been also compared with corresponding ones for the GaN(110) surface, for which a very good agreement with other calculations is found. Different features in the RA spectra are found between the nitrides surfaces and the GaAs(110). For GaN(110) a negative structure takes place at the onset of its RA spectrum, confirming previous tight-binding results. For surface optical properties of BN(110) the present results are the first *ab initio* ones. A fundamental role at the onset of the RA spectrum of this system is played by transitions between surface states. Both nitrides surfaces display stronger structures at the onset of their RA spectra with respect to those appearing in the case of the less ionic system GaAs(110).

#### ACKNOWLEDGMENTS

The authors would like to thank O. Pulci and R. Del Sole for helpful discussions. This work has been supported by the ENEA Computing Environment at Centro Ricerche ENEA, Casaccia (Rome). Support from INFN through the PRA project IMESS is also acknowledged.

\*Present address: INFN and Dipartimento di Fisica dell'Università di Milano, via Celoria 16, I-20133, Milano, Italy.

<sup>1</sup>*Synthesis and Properties of Boron Nitride*, edited by J.J. Pouch and S.A. Alterovitz (Trans. Tech. Aedermannsdorf, 1990).

<sup>2</sup>*Properties of Group III Nitrides*, edited by J.H. Edgar (Kansas State University, Kansas, 1994).

<sup>3</sup>*Group III Nitride Semiconductors Compounds: Physics and Applications*, edited by B. Gil (Oxford Science, London, 1998).

<sup>4</sup>M.A. Herman and H. Sitter, *Molecular Beam Epitaxy* (Springer, Berlin, 1993).

<sup>5</sup>R. Del Sole, *Reflectance Spectroscopy-Theory*, edited by P. Halevi, Photonic Probes at Surfaces (Elsevier Science, Amsterdam, 1995), pp. 133–173.

<sup>6</sup>L. Kleinmann and J.C. Phillips, Phys. Rev. **117**, 460 (1960).

<sup>7</sup>E. Doni and G. Pastori Parravicini, Nuovo Cimento B **64**, 117 (1969).

<sup>8</sup>H.R. Philipp and E.A. Taft, Phys. Rev. **127**, 159 (1962).

<sup>9</sup>X. Blase, A. Rubio, S.G. Louie, and M.L. Cohen, Europhys. Lett. **28**, 335 (1994), Phys. Rev. B **28**, 6868 (1995).

<sup>10</sup>M.I. Eremets, K. Takemura, H. Yusa, D. Goldberg, Y. Bando, V.D. Blank, Y. Sato, and K. Watanabe, Phys. Rev. B **57**, 5655 (1998).

<sup>11</sup>M. Sokolowski, J. Cryst. Growth **46**, 136 (1979).

<sup>12</sup>G. Kern, G. Kresse, and J. Hafner, Phys. Rev. B **59**, 8551 (1999).

<sup>13</sup>D.M. Hoffman, G.L. Doll, and P.C. Eklund, Phys. Rev. B **30**, 6051 (1984).

<sup>14</sup>R.M. Chrenko, Solid State Commun. **14**, 511 (1974).

<sup>15</sup>G. Cappellini, V. Fiorentini, K. Tenelsen, and F. Bechstedt, in *Gallium Nitride and Related Materials*, edited by R. D. Dupuis, J.A. Edmond, F.A. Ponce, and S. Nakamura, Mater. Res. Soc. Symp. Proc. No. **395** (Materials Research Society, Pittsburg, 1996), p. 429.

<sup>16</sup>M.P. Suhr, S.G. Louie, and M.L. Cohen, Phys. Rev. B **43**, 9126 (1991).

<sup>17</sup>G. Cappellini, G. Satta, M. Palummo, and G. Onida, Phys. Rev. B **43**, 9126 (2001).

<sup>18</sup>F. Manghi, R. Del Sole, A. Selloni, and E. Molinari, Phys. Rev. B **41**, 9935 (1990).

<sup>19</sup>J. Yamauchi, M. Tsukada, S. Watanabe, and O. Sugino, Surf. Sci. **341**, L1037 (1995).

<sup>20</sup>J. Yamauchi, M. Tsukada, S. Watanabe, and O. Sugino, Phys. Rev. B **54**, 5586 (1996).

<sup>21</sup>K. Kàdas, G. Kern, and J. Hafner, Phys. Rev. B **58**, 15 636 (1998).

<sup>22</sup>K. Kàdas, G. Kern, and J. Hafner, Phys. Rev. B **60**, 8719 (1999).

<sup>23</sup>O. Pulci, G. Onida, R. Del Sole, and L. Reining, Phys. Rev. Lett. **81**, 5374 (1998).

<sup>24</sup>C. Noguez, Phys. Rev. B **62**, 2681 (2000).

- <sup>25</sup>R.M. Dreizel and E.K.U. Gross, *Density Functional Theory* (Springer, New York, 1990).
- <sup>26</sup>J.P. Perdew and A. Zunger, Phys. Rev. B **23**, 5048 (1981).
- <sup>27</sup>D.M. Ceperley and B.J. Alder, Phys. Rev. Lett. **45**, 566 (1980).
- <sup>28</sup>X. Gonze, R. Stumpf, and M. Scheffler, Phys. Rev. B **44**, 8503 (1991).
- <sup>29</sup>M. Fuchs and M. Scheffler, Comput. Phys. Commun. **119**, 67 (1999).
- <sup>30</sup>N. Troullier and J. L. Martins, Phys. Rev. B **43**, 1993 (1991).
- <sup>31</sup>S.G. Louie, S. Froyen, and M.L. Cohen, Phys. Rev. B **26**, 1738 (1982).
- <sup>32</sup>O. Pulci, G. Onida, A.I. Shkrebtii, R. Del Sole, and B. Adolph, Phys. Rev. B **55**, 6685 (1997).
- <sup>33</sup>D.J. Chadi and M.L. Cohen, Phys. Rev. B **8**, 5747 (1973).
- <sup>34</sup>R. Miotto, G.P. Srivastava, and A.C. Ferraz, Surf. Sci. **426**, 75 (1999).
- <sup>35</sup>A. Filippetti, V. Fiorentini, G. Cappellini, and A. Bosin, Phys. Rev. B **59**, 8026 (1999).
- <sup>36</sup>U. Grossner, J. Furthmüller, and F. Bechstedt, Phys. Rev. B **58**, 1722 (1998).
- <sup>37</sup>J.E. Northrup, and J. Neugebauer, Phys. Rev. B **53**, R10 477 (1996).
- <sup>38</sup>X. Zhu, S.B. Zhang, S.G. Louie, and M.L. Cohen, Phys. Rev. Lett. **63**, 2112 (1989).
- <sup>39</sup>B. Adolph, V.I. Gavrilenko, K. Tenelsen, F. Bechstedt, and R. Del Sole, Phys. Rev. B **53**, 9797 (1996).
- <sup>40</sup>A.F. Starace, Phys. Rev. A **3**, 1242 (1977).
- <sup>41</sup>O. Pulci, G. Onida, R. Del Sole, and A. Shkrebtii, Phys. Rev. B **58**, 1922 (1998).
- <sup>42</sup>M.S. Hybertsen and S.G. Louie, Phys. Rev. B **34**, 5390 (1986).
- <sup>43</sup>F. Bechstedt, *Festkörperprobleme-Advances in Solid State Physics*, edited by U. Rössler (Vieweg, Braunschweig/Wiesbaden, 1992), Vol. 32, p. 161.
- <sup>44</sup>F. Bechstedt and R. Del Sole, Phys. Rev. B **38**, 7710 (1988).
- <sup>45</sup>F. Gygi and A. Baldereschi, Phys. Rev. Lett. **62**, 2160 (1989).
- <sup>46</sup>L. Hedin, Phys. Rev. **139**, A796 (1965); L. Hedin and S. Lundqvist, Solid State Phys. **23**, 1 (1969).
- <sup>47</sup>R. Godby, M. Schlüter, and L.J. Sham, Phys. Rev. B **37**, 10 159 (1988).
- <sup>48</sup>V.I. Gavrilenko and R.Q. Wu, Phys. Rev. B **61**, 2632 (2000).
- <sup>49</sup>Y.-N. Xu and W.Y. Ching, Phys. Rev. B **48**, 4335 (1993).
- <sup>50</sup>W.R. Lambrecht, B. Segall, S. Strite, G. Martin, A. Agarwal, H. Morkoc, and A. Rocket, Phys. Rev. B **50**, 14 155 (1994).
- <sup>51</sup>W.R. Lambrecht, B. Segall, J. Rife, W.R. Hunter, and D.K. Wickenden, Phys. Rev. B **51**, 13 516 (1995).
- <sup>52</sup>V. Fiorentini, M. Methfessel, and M. Scheffler, Phys. Rev. B **47**, 13 353 (1993).
- <sup>53</sup>F. Bechstedt, O. Pulci, and W.G. Schmidt, Phys. Status Solidi A **175**, 5 (1999).